Advanced Motion Control for Safe Navigation of an Omnidirectional Wall-Climbing Robot

Daniel Schmidt* and Karsten Berns

Robotics Research Lab, Department of Computer Sciences, University of Kaiserslautern,
67663 Kaiserslautern, Germany, *E-mail: dschmidt@cs.uni-kl.de

Abstract. Safe navigation a great challenge for wall-climbing robots which adhere to the surface via negative pressure. Especially wheeled systems which are able to drive on vertical concrete structures like bridge pylons or dams need special measures to enhance safety. This paper presents the advanced motion control system of the climbing robot CROMSCI which uses a negative pressure adhesion system in combination with driven wheels for propulsion. The main demands to this motion control system related to robot safety are to enhance the transferable force in driving direction, reduce the wear of wheels and to minimize the chance of robot slip. This can be achieved via special traction control components and additional elements as presented in this paper. Experimental results prove the operability of the described measures.

1 Introduction

For wall-climbing robots safety is a main requirement. Therefore, developers spend much effort in methods which increase the safety of these systems. In contrast to ground vehicles climbing robots are relatively slow and do not interact with humans – so the most endangered object is the robot itself. The problem of safe navigation is manageable if the climbing robots use legs for propulsion with independent adhesion units like suction cups or claws [ABC05,SHS+08]. Here one can position the foot at the desired point and test the grip [LCC+01]. Either the adhesion is sufficient and the robot can continue or it has to find a more suitable position and test further touchdown points. Other robots use very safe adhesion systems like magnets [SBS+08] which will not fail on the individual surface or are so light weighted that they do not have to take care for these problems [KST07,PPS08]. The disadvantage of these systems is the very limited payload respective the restriction to ferromagnetic surfaces.

One application for robots which are able to climb on vertical concrete structures are inspection tasks of buildings like cooling towers or bridge pylons. Legs or sliding frame mechanisms for locomotion result in slow and rugged movement which is not applicable for these tasks, since suitable systems need a sufficient fast navigation between inspection points and the ability of carrying a high payload in terms of inspection sensors. Therefore, a drive system seems to be the best solution to achieve a fast and continuous motion and allow a more simple mechanical structure. But for robots climbing on concrete walls via negative pressure adhesion in combination with a drive system the stress on the popultion system is an aspect which can not be neglected. Wheeled

system have the disadvantage of wheel wear due to wheelslip and lateral forces and are endangered to start slipping. These problems can be reduced by using methods of traction control and similar measures.

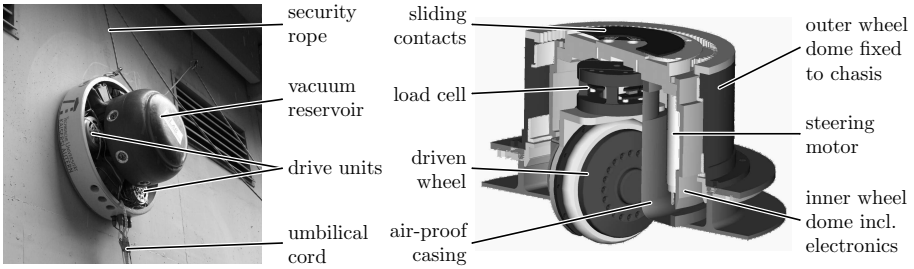

Fig. 1. Climbing robot CROMSCI at a concrete wall (left) and a drive unit for propulsion (right).

This research is focused on climbing robot CROMSCI as depicted in figure 1 (left) which is demanded to inspect large concrete buildings even overhead. Therefore, it needs a relatively high velocity in all directions. The robot can be equipped with a movable manipulator arm to carry inspection sensors like impact echo, cover meter or a Wenner probe. For communication purposes and energy supply it is connected to a ground station via an umbilical cord. The unique feature of CROMSCI is the negative pressure system consisting of seven individual adhesion chambers in a shape of spokes which allows a balancing of downforces [SHB11]. Three suction engines evacuate a vacuum reservoir on top which is connected via valves to the adhesion chambers at the undercarriage. Inflatable chamber sealings glide over the surface and make the system more or less air-proof. The total weight of the robot is 45 kg with an additional payload of up to 10 kg. The diameter of the chassis is 80 cm. For locomotion the robot uses three unsprung and driven steerable standard wheels as depicted in figure 1 (right) which allow a high maneuverability and fast and continuous motion with a maximum speed of 9.63 m/min. Load cells have been integrated into the wheel units to measure forces and torques at the contact point between wall and wheel.

The following section 2 will describe the single components of the advanced motion control system and its final setup. Experimental results follow in section 3. Finally, section 4 will summarize the findings.

2 Advanced Motion Control

The task is now to fulfill the given safety requirements since the robot should not only adhere to the wall but also move on it. In general, one can distinguish three control layers which are considered here. The *planning layer* on top contains the forward and backward kinematics of the omnidirectional drive and adaptions of these control values (section 2.1). The *reactive layer* in between adapts desired orientations and velocities to reduce shear forces as shown in section 2.3. The *basic layer* consists of three DSP boards

(one per wheel unit) which are connected via CAN-bus to the PC. They contain basic closed-loop motion controllers to adjust position or velocity and the traction control system as described in section 2.2.

2.1 Ambiguities and Boundary Conditions

Based on kinematic calculations [SHB11] desired steering and turning commands for the wheel controllers can be determined. But as in most cases the results from the inverse kinematic are not unique. It is obvious, that there exists an unlimited number of possible steering orientations due to the fact that the wheel domes can turn endlessly. Furthermore it is possible to rotate in both directions to reach a specific position. To handle these ambiguities one has to use boundary conditions which also have a positive effect on navigation safety.

An evident measure is the **minimization of steering**. The first option to reduce steering is to turn the shortest way (left or right) depending on the actual wheel dome orientation. The resulting motion can be $\pm 180^\circ$ in the worst case. The second option is to inverse the wheel's rotation direction if necessary which lowers the worst-case to $\pm 90^\circ$ turning. To find the shortest turning angle of wheel Wi the actual steering value has to be split into the actual amount of overturning $\Phi_{Wi}^{act} \in \mathbb{N}$ and the current angle $\varphi_{Wi}^{act} \in [-\pi, \pi)$ due to the fact that the desired value from the kinematics is given in the range of $[-\pi, \pi)$. Depending on the desired turning distance one of four possibilities (steer left/right and drive forward/backward) is chosen for the wheel controller.

A second measure related to the drive kinematics is to **avoid wheel turning onto the point**. If the desired wheel velocity v_{Wi}^{des} is zero the wheel does not contribute anything to robot motion. In this case the target steering angle φ_{Wi}^{des} is set to the actual one φ_{Wi}^{act} which keeps the wheel dome in its current orientation. The benefit is the reduction of unwanted wheel slip e.g. if the drive system transfers from straight driving to full turning and robot only steers but does not move. Results are presented later in section 3.

2.2 Traction Control System

As already mentioned wheeled systems have a general problem of wheelslip which increases, if the robot is going upwards a vertical wall and has to overcome gravity. The *reduction of wheel slip* is one important method to fulfill safety requirement related to a reduction of wheel abrasion and of an enhanced robot movement. General traction control systems (TCS) are a well known field in industry and robotics [ZC10]. An overview concerning different traction control systems applied at automobiles can be found at [Bur93]. But based on the present system setup, a novel slip reduction technique has been developed which uses measured forces at the wheel contact point [SHB11] since classic approaches are not suitable in this special context.

In a physical sense a loss of traction is the result of too low friction force compared to affecting lateral and tangential forces at the contact point between wall and wheel as in general describe in terms of a friction circle. The maximum transferable force in rolling direction $F_{Wi|x}^{max}$ can be estimated according to equation 1 based on an estimated static friction value $\hat{\mu}_{stat}$, the actual downforce $F_{Wi|z}^{act}$ and the sideward force $F_{Wi|y}^{act}$ which are measured by the integrated load cell:

$$F_{Wi|x}^{max} = \sqrt{(\hat{\mu}_{stat} \cdot F_{Wi|z}^{act})^2 - (F_{Wi|y}^{act})^2} \tag{1}$$

The traction control system runs on the DSP boards and adjusts the wheel propulsion if the actual force in driving direction reaches a specific percentage of this maximum. At first the actual PWM limit $I_{Wi|v}^{max}$ of wheel Wi is trimmed according to equation 2. The former maximum $I_{Wi|v}^{max\prime}$ is enhanced by two constant update factors with $I_p << I_m$ depending on the comparison of actual $F_{Wi|x}^{act}$ and maximal transferable force $F_{Wi|x}^{max}$. In application, the wheel propulsion is reduced fast in case of wheel slip whereas it recovers much slower to the normal level. $I_{Wi|v}^{low}$ and $I_{Wi|v}^{up}$ are constant lower and upper limits of the PWM value to assure a minimum of energy in the one and to prevent an overstraining in the other case.

$$I_{Wi|v}^{max} = \begin{cases} I_{Wi|v}^{max\prime} - I_m & \text{, if } F_{Wi|x}^{act} > F_{Wi|x}^{max} \wedge I_{Wi|v}^{max\prime} > I_{Wi|v}^{low} \\ I_{Wi|v}^{max\prime} + I_p & \text{, if } F_{Wi|x}^{act} < F_{Wi|x}^{max} \wedge I_{Wi|v}^{max\prime} < I_{Wi|v}^{up} \\ I_{Wi|v}^{max\prime} & \text{, else} \end{cases} \tag{2}$$

Afterwards, this maximum is used to limit the PWM value for locomotion $I_{Wi|v}$ to the range of $[-I_{Wi|v}^{max}, I_{Wi|v}^{max}]$. Finally, the integral value $I_{Wi|v,\mathrm{I}}$ of the PI motor velocity controller has to be adapted during limitation of the motor current to avoid further increases of the integral portion [SHB11]. The controller setup is illustrated in figure 2.

2.3 Shear Force Controlling

As shown in equation 1 the maximum transferable force in rolling direction $F_{Wi|x}^{max}$ of a wheel is affected by the downforce and by sideward forces $F_{Wi|y}^{act}$ in y-direction of the wheel. These unmeant forces can occur because of steering transitions, incorrect initializing or runtime errors of the turning wheel domes and should be avoided. Beside the greater risk of slip these shear forces also have a negative effect on wheel abrasion and on the mechanical structure of the drive units.

To *decrease shear forces* the actual force values of each wheel F_{Wi}^{act} and its orientation φ_{Wi}^{act} are transfered to the *reactive layer* on the PC. The first step is to calculate desired forces for each wheel depending on the percentage of current downforce $F_{Wi|z}^{act}$ compared to total downforce (equation 3):

$$\begin{pmatrix} F_{Wi|x}^{des} \\ F_{Wi|y}^{des} \end{pmatrix} = \frac{F_{Wi|z}^{act}}{\sum_{j=1}^{3} F_{Wj|z}^{act}} \cdot R(-\varphi_{Wi}^{act}) \cdot \sum_{j=1}^{3} R(\varphi_{Wj}^{act}) \cdot \begin{pmatrix} F_{Wj|x}^{act} \\ F_{Wj|y}^{act} \end{pmatrix} \tag{3}$$

The forces in y-direction can now be reduced by adapting the steering angles via a PI-similar controller with amplification parameters $K_{\mathrm{SFC}|\varphi,\mathrm{P}}$, $K_{\mathrm{SFC}|\varphi,\mathrm{I}}$ and an initial downforce $F_{R|z}^{init}$. The desired values φ_{Wi} are adapted by a proportional and an integral offset as shown in equation 4. The forces in rolling direction can be reduced in the same way

by calculating velocities offsets v_{Wi}^{offset} which depend on $F_{Wi|x}^{act}$ instead of the forces in y-direction. The final steering and velocity values are determined by adding the offset values to the desired commands from the kinematic calculation.

$$\begin{aligned} \varphi_{Wi}^{offset}(t) = & K_{\text{SFC}|\varphi,\text{P}} \cdot \frac{F_{R|z}^{init}}{F_{Wi|z}^{act}} \cdot \left(F_{Wi|y}^{des}(t) - F_{Wi|y}^{act}(t) \right) \quad \Big\} \text{ proportional portion} \\ & + K_{\text{SFC}|\varphi,\text{I}} \cdot \frac{F_{R|z}^{init}}{F_{Wi|z}^{act}} \cdot \sum_{\tau=1}^{t} \left(F_{Wi|y}^{des}(\tau) - F_{Wi|y}^{act}(\tau) \right) \Big\} \text{ integral portion} \end{aligned} \tag{4}$$

2.4 Final Controller Setup

Figure 2 shows the final setup of TCS and SFC. The desired steering and driving commands φ_{Wi} and v_{Wi} from the kinematics considering the boundary conditions from section 2.1 are adapted by the SFC based on actual downforce values. Each of the three DSP circuit boards is responsible for one drive unit. The motor controllers with successional motor electronics and amplyfiers generate PWM signals for steer and drive motors. Based on the estimated friction value $\hat{\mu}_{stat}$ and actual force values the PWM value of the motor for locomotion is limited to $I_{Wi|v}^{max}$ by the TCS.

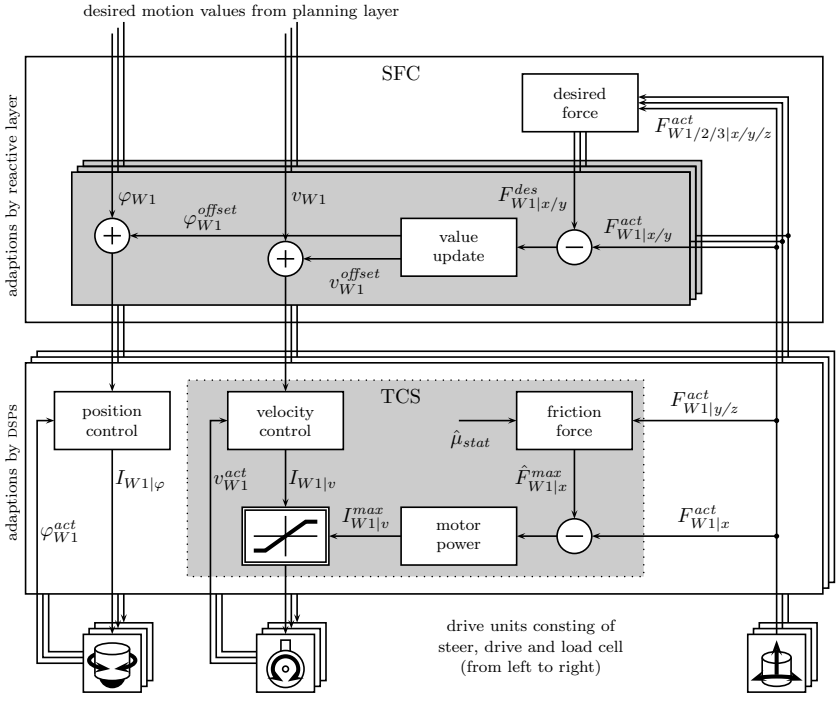

Fig. 2. Detailed view of the lower AMC elements traction and shear force control.

3 Results and Impact on Navigation Safety

The **boundary measures** – no turning onto the point and minimized steering – affect robot safety in a way that they reduce wear of the wheels and replaces dynamic friction by static friction in some situations. Figure 3 shows the benefit of the avoidance of steering onto the point. Here, the robot has been pulled manually two times on the ground and the sideward forces have been measured. In the first case the wheel domes were rotating to simulate a steering onto the point whereas the wheels were set fixed in a second test run. One can see, that turning onto the point reduces the required pulling force to 86 % of its maximum which raises the chance of robot slip in the same manner.

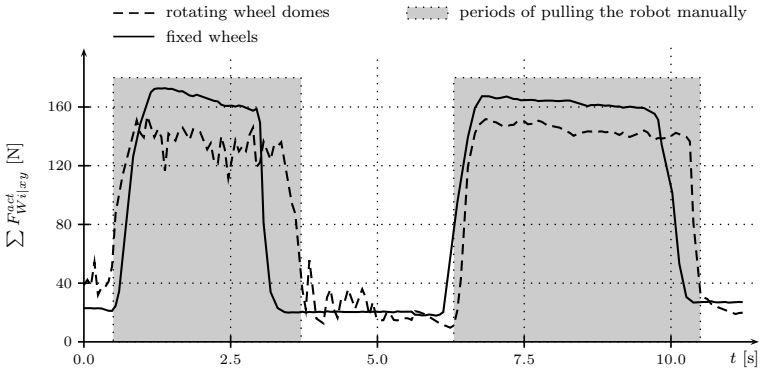

Fig. 3. Needed sideward forces to pull the robot by hand. In average the force is lowered from about 159.9 N (solid line) to 137.5 N if the wheel domes are turning (dashed line).

To test the benefit of the **traction control system** the robot moves upwards a wall with immediate accelerations. It already has been proven that the robot is able to drive up to eight times further with activated TCS compared to test runs with disabled traction control [SHB11]. Regarding navigation safety, figure 4 shows the ratio of sideward forces $F_{W1|xy}$ to the absolute downforce $F_{W1|z}$ of the front wheel. This ratio (equation 5) is very interesting due to the fact that it allows a conclusion of dangerous slipping of the robot and can be determined based on equation 1. It describes, how large the static friction value must be at minimum to be able to transfer the sideward forces. If this inequality is not fulfilled the wheel will start slipping. In the example given in figure 4 the ratio was enhanced by the TCS, but stayed below the used estimated friction coefficient $\hat{\mu}_{stat} = 0.8$ in both cases.

$$\mu_{stat} \geq \frac{F_{Wi|xy}}{F_{Wi|z}} = \frac{\sqrt{(F_{Wi|x})^2 + (F_{Wi|y})^2}}{F_{Wi|z}} \tag{5}$$

Additionally, further experiments have shown that the drive control without TCS always reaches the maximum pulse width modulation (PWM) value of 20,000 while

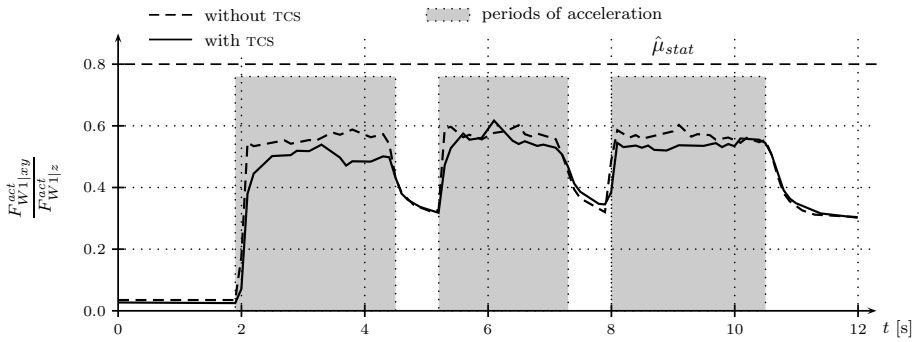

Fig. 4. Ratio of sideward forces to downforce of front wheel which has been enhanced from an average value of 0.56 during the three motion phases to 0.52 with activated traction control system.

moving up whereas they lie between $16,000$ and $17,000$ with activated TCS. One has to keep in mind that this traction control enables the robot to move further with less motor current. Nevertheless, it is obvious that the traction control system can not annul physics and a general wheel slip during continuous motion – especially in upward direction – can not be avoided. But remember: even cars have a general wheel slip of 10 to 20% on dry asphalt without overcoming gravity.

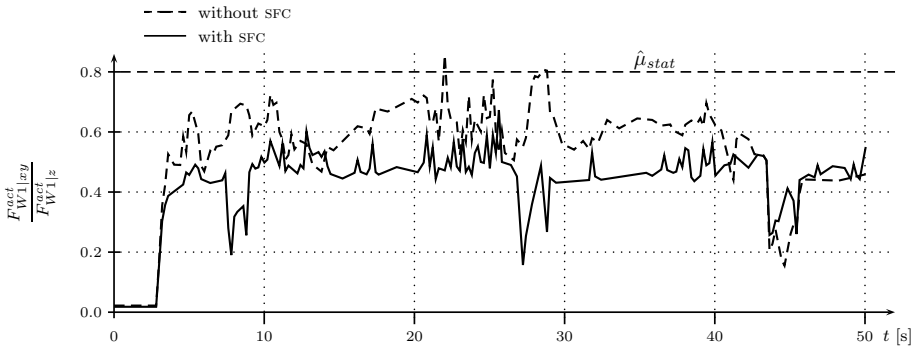

Fig. 5. Ratio of sideward forces to downforces while moving up a wall with permanently changing velocity and direction commands – with (solid line) and without (dashed line) shear force control. The SFC reduces this ratio significantly.

The first experiments with the **shear force controller** have been executed on flat ground. This setup has been chosen to exclude additional sideward forces e.g. based on gravity which affect the measurements. In average these shear forces are reduced by 63.2% via the introduced SFC. Further experiments were executed at a vertical wall with many motion changes which produced a lot of shear forces as illustrated in figure 5.

The plots show the ratio of sideward forces $F_{W1|xy}$ to the absolute downforce $F_{W1|z}$ of the front wheel as already used in case of the TCS (see equation 5). The average ratio is reduced from 0.543 to 0.429 by the SFC. Even better is the result, that this ratio remains below the estimated friction value $\hat{\mu}_{stat}$. This experiment shows the great importance of this measure to enhance robot adhesion and navigation safety.

4 Conclusion

This paper presented a couple of components for advanced motion control to enhance navigation safety of a wall-climbing robot including traction control, shear force control and additional kinematical adaptions. The advantages of the presented measures for robot safety have been shown in experiments and can be summed up as follows: Increased lifetime of wheel rubber (less wheel slip), of wheel mechanics (lower sideward forces) and of drive motors (lower permanent current). Decreased chance of robot slip due to reduced wheel slip and better transfer of holding and motion forces. Finally one receives a reduced time in operation because of faster robot motion.

Current development is focused on an enhanced mechanical structure, since the potential of optimization using control components seems to be exhausted. This includes a more lightweighted robot chassis which decreases the required motion forces and an optimized wheel rubber to improve the friction between wheel and wall.

References

[ABC05] K. Autumn, M. Buehler, and M. Cutkosky et al. Robotics in scansorial environments. In *SPIE - The International Society for Optical Engineering*, volume 5804, May 2005.

[Bur93] M. Burckhardt. *Fahrwerktechnik: Radschlupf-Regelsysteme*. Vogel Buchverlag, 1993.

[KST07] S. Kim, M. Spenko, and S. Trujillo et al. Whole body adhesion: hierarchical, directional and distributed control of adhesive forces for a climbing robot. In *IEEE International Conference on Robotics and Automation*, April 2007.

[LCC+01] B. L. Luk, D. S. Cooke, A. A. Collie, N. D. Hewer, and S. Chen. Intelligent Legged Climbing Service Robot For Remote Inspection And Maintenance In Hazardous Environments 1. In *8th IEEE Conference on Mechatronics and Machine Vision in Practice*, pages 252–256, 2001.

[PPS08] H. Prahlad, R. Pelrine, and S. Stanford et al. Electroadhesive robots - wall climbing robots enabled by a novel, robust and electrically controllable adhesion technology. In *International Conference on Robotics and Automation (ICRA)*, May 19-23 2008.

[SBS+08] J. Shang, B. Bridge, T. Sattar, S. Mondal, and A. Brenner. Development of a climbing robot for inspection of long weld lines. *Industrial Robot: An International Journal*, 35(3):217–223, 2008.

[SHB11] D Schmidt, C Hillenbrand, and K Berns. Omnidirectional locomotion and traction control of the wheel-driven, wall-climbing robot, Cromsci. *Robotica Journal*, 29(7):991–1003, 2011.

[SHS+08] M.J. Spenko, G.C. Haynes, J.A. Saunders, M.R. Cutkosky, A.A. Rizzi, and D.E. Koditschek. Biologically inspired climbing with a hexapedal robot. *Journal of Field Robotics*, 25(4-5):223–242, 2008.

[ZC10] T Zielinska and A Chmielniak. Controlling the slip in mobile robots. In *13th International Conference on Climbing and Walking Robots (CLAWAR)*, number 4 in 1, pages 13–20, 2010.